Cleaner Materials 11 (2024) 100215

Contents lists available at ScienceDirect

Cleaner Materials

journal homepage: www.journals.elsevier.com/cleaner-materials

Estimating attached mortar paste on the surface of recycled aggregates based on deep learning and mineralogical models

Andrea Bisciotti [a,*], Derek Jiang [b], Yu Song [b,*], Giuseppe Cruciani [a]

[a] University of Ferrara, Department of Physics and Earth Science, Via Saragat 1, 44141 Ferrara, Italy
[b] University of California Los Angeles, Department of Civil and Environmental Engineering, Physics of AmoRphous and Inorganic Solids Lab (PARISlab), 520 Portola Plaza, Los Angeles, CA, 90095, USA

ARTICLE INFO

Keywords:
Recycled aggregates
Attached mortar
C&DW
Machine learning
X-ray diffraction

ABSTRACT

Recycled aggregates, obtained from construction and demolition waste (C&DW), are currently underutilized in the production of new concrete given the incidence of widespread leftover cement paste adhering to the surface. C&DW sorting facilities based on optical technology can be developed and applied on an industrial scale, improving the overall quality of this secondary raw material. In this study, we present a novel approach based on image analysis and mineralogical laboratory methods to determine the residual attached mortar volume. Through clustering analysis, we classify C&DW samples with a comparable cement content determined by the image analysis. The leftover cement paste from these C&DW classes is mechanically extracted and examined using X-ray Powder Diffraction and Rietveld refinement. To estimate the attached mortar volume and the carbonation of the cement paste, we present a novel mathematical model based on the mineralogical data. To overcome the bottleneck associate with the image analysis, we further incorporate a deep learning model to automate the determination of the mortar volume, which enables high-throughput screening of C&DW in real production.

1. Introduction

One of the most important steps toward achieving the circular economy in the construction industry is recycling and reusing construction and demolition waste (C&DW) in the production of new concrete and new building materials. Recent literature identified at least two different types of recycled aggregates (RAs) which can be recovered from C&DW (Silva et al., 2014): (1) Mixed Recycled Aggregates, and (2) Recycled Concrete Aggregates. The latter is directly derived from the comminution of C&DW containing more than 90% of concrete. It is commonly acknowledged that RAs made from C&DW crushed concrete have the potential to substitute natural aggregates (NA) in construction projects (Fan et al., 2016; Wang et al., 2021a). This latter, compared to NA, can be often distinguished by the presence of residual cement paste bound to their surface. Due to its chemical composition, the attached mortar interacts with cementitious binders, forming a thin layer known as the interfacial transition zone in the area of surface contact. As a result of this effect, integrating RAs instead of NA often leads to inferior mechanical performances and reduced workability in the new concrete, depending on the amount of AM (Bai et al., 2020; H. Zhang et al., 2022). The addition of fibers (fiber-reinforced recycled aggregate concrete) represents a viable solution to inhibit the coalescence of the weak areas of the interface transition zone, at the same time their use is not always suitable in every engineering application due to costs and operating conditions (Wang et al., 2022a; Wang et al., 2022b).

Besides the pure content of residual cement paste attached to the C&DW aggregate, the bulk assemblage and composition of the residual cement itself has direct impact to define the correct and most efficient managing strategy to reuse RAs facing the AM impact. The composition of the attached mortar can be very diverse due to various aging, environmental circumstances during disposal, and the initial composition of the cement used. Mostly, the carbonation level of the residual paste attached has a significant impact on varying the mineralogical major phases (Georget et al., 2020; Shen et al., 2022). Therefore, the degree of carbonation of the layer itself also affects, together with the amount of AM, the possibility of reusing RAs in new cement paste (Lu et al., 2019; R. Wang et al., 2020).

Because of the variability of the C&DW properties, these secondary raw-materials are currently underutilized in the manufacturing of new concrete, whilst they are mostly used for esplanades or as sub-bases and

---

* Corresponding authors.
E-mail addresses: bscndr@unife.it (A. Bisciotti), yusong@ucla.edu (Y. Song).

https://doi.org/10.1016/j.clema.2023.100215
Received 16 August 2023; Received in revised form 13 December 2023; Accepted 18 December 2023

bases of pavements/roads and highways. This can be labeled as downcycling and greatly hinders the industry's potential to transition to a circular economy since the net expansion of the road infrastructure is reducing and may eventually come to an end (C. Zhang et al., 2020).

In the present scenario, C&DW concrete recycling relies mostly on industrial crushing and sieving techniques, often using jaw crushers and impact crushers in order to produce an unsorted granular product with the necessary size fractions (Ulsen et al., 2019). Mixed C&DW streams will have to be separated and extensively cleaned up before comminution, in order to gain enough quality to reuse the different fractions. After conducing primary, and occasionally secondary crushing, an electromagnet is usually employed to remove any metallic components (such as rebars). Nevertheless, coarse RAs, obtained from recycled concrete, are often discharged because they still have residual cement paste clinging to the surface, despite being successfully sorted within C&DW. A step forward in sorting strategies, has just recently been outlined and discussed for the fine C&DW materials (<4 mm) based on mechanical system for extracting the RAs separating the cement-based fractions (Gebremariam et al., 2020).

The development of advanced separation process for C&DW can improve the quality of this secondary raw material, reducing the overall heterogeneity, and enhancing the effectiveness of the reuse of these products in substitution to natural aggregates counterparts in concrete production. Optical sorting is one of the most advanced key technology for the coarse C&DW fractions (≥4 mm), even if still not extensively adopted world-wide in C&DW treatment plants (J. Li et al., 2022; Nežerka et al., 2024; Serranti et al., 2023). Therefore, to meet the efficient sorting of C&DW in industrial plants, advanced sorting-machine can be used for screening high-quality RAs, based on AM content, using RGB optical sensors and hyper-spectral imaging cameras (Bonifazi et al., 2018; Trotta et al., 2021). In order to increase performance, this strategy also needs a significant contribution from machine learning, specifically deep neural networks (DNN), which classify the acquired data (RGB or hyper-spectral) in agreement with the material composition (Lau Hiu Hoong et al., 2020).

The separation and further quantification of AM appears then as mandatory processes to assess the quality of RAs, and different methods have been proposed (mechanical, thermal, thermal–mechanical, chemical, microwave, ultra-sound) as summarized in (Braymand et al., 2017; Tam et al., 2021). In spite of those methods, an internationally standardized procedure has not been established yet.

The quantification of AM based on image analysis methods (IAM) using digital cameras has been one of the early achievements in RAs scientific researches (Abbas et al., 2009; Ulsen et al., 2022; Wang et al., 2021b). However, a bottleneck of the conventional IAM lies in the fact that this approach can be very sensitive to noise artifacts and blurring (Singh, 2015). In addition, segmenting the attached mortar in the image often requires constant human judgments (e.g., for readjusting the color threshold even when there is a slight change in the aggregate type or light conditions). Hence, despite the advances of conventional image analysis in recognizing the residue mortar, it is challenging to use this approach to overcome the above limitations for fulfilling high-throughput screening of recycled aggregates in real engineering projects.

Alternatively, recent advances in artificial intelligence (AI) and computer vision open up new opportunities to rely on a computer to accomplish vision-based tasks such as object recognition or image perception (Pan & Zhang, 2021; Szeliski, 2022). This approach has been demonstrated to be successful in multiple fields in civil engineering (Xu et al., 2021) including phase analysis for concrete materials (Das et al., 2022; Song et al., 2020). The rationale behind this approach is that AI is good at capturing the correlation between the input data and the predicted target, including the explicit information that is utilized by the image analysis (e.g., color contrast) but also some implicit clues that may not be easily captured (e.g., material texture). To the best of our knowledge, however, the potential of AI has not been investigated for improving the detection of the residue mortar in recycled aggregates.

To overcome the challenges associated with conventional image analysis, we leverage AI and computer vision techniques to enable a direct and robust inference of the residual mortar attached to the aggregate. To this end, a deep learning model is developed to leverage the advances of convolutional neural network (CNN) in recognition of the different phases in the aggregate image. In particular, our model is trained to predict the mass fraction of the AM on the recycled aggregate particles.

In addition to determining the AM content, a quick, accurate, and repeatable method is provided to determine the RA's degree of carbonation in order to categorize the C&DW and stimulate the final reuse. There are several methods for quickly evaluating the carbonation of concrete, but RAs specimens are unable to be utilized within the same measurements. To obtain accurate information on the carbonation front, laboratory tests are typically conducted (Georget et al., 2020; Tang et al., 2023) and usually combine scanning electron microscopy (SEM), X-ray diffraction (XRD), and thermogravimetric analysis (TGA). Even though they are highly accurate, these approaches are not appropriate for a quick evaluation of the carbonation degree.

A novel mathematical model based on the outcomes of X-ray powder diffraction analysis is introduced for the first time in in order to categorize the RAs based on a bulk volume materials reconstruction. As parameters to the equation, we propose quantitative phase analysis outcome, which is based on Rietveld modeling of diffraction patterns together with tabular mineral phase density data.

Such a method has the potential to be industrially applied to quality control, as it has already been proposed in the mining industry to estimate the main parameters of minerals grade ore deposits as a faster and cheaper alternative to traditional wet chemistry methods, ensuring reproducibility and accuracy of prediction even when the ore feeding the plant is changed. (Melo et al., 2020; Mulder et al., 2013). The Rietveld approach is already well-established in the field of cement research for developing prediction models of newly-formed mineral assemblages in the kiln and in the hydration process. (Abzaev et al., 2019; Mulder et al., 2013). The contribution in the field of C&DW is presented here for the first time.

The identified hydrated minerals and anhydrous cement components, after only using XRPD, give a detailed in-deep description of the C&DW and a direct evaluation of the carbonation level of the connected cement paste. The output consists of a 3D volume reconstruction of the associated AM and on a direct assessment of the degree of carbonation of the layer resulting from the bulk microscopic crystalline mineralogical assemblage.

The output of the research represents an innovative approach to determining the most effective strategies for the reuse of concrete-based C&DW based on the estimation of AM content and carbonation degree of the connected residual cement paste.

2. Materials and methods

2.1. Materials

The C&DW acquired from a precasting facility in Perugia (Umbria District, Italy) was jaw-crushed on an industrial scale to produce the RAs under analysis. The crusher's parameters were defined to produce aggregates with a diameter between 0 and 25 mm. For this reason, the jaw spacing was fixed at 22 mm for the jaw crusher, accordingly to a previous work (Hubert et al., 2023). The beginning C&DW comprises more than 90% structural concrete (>40 MPa), resulting in a product that may be categorized as recycled concrete aggregates. (Silva et al., 2014). The collection of material samples followed the guidelines in standard UNE-EN 932–1, 1997. The RAs are homogenized and decreased in the lab using a quartering process according to UNE-EN 932–2, 1999. Following screening, an average of 70% of the material produced by industrial jaw-crushing of C&DW is formed of the coarse fraction of RAs (≥4 mm), which is also the granulometric diameter with the greatest potential for recycling. (Pedro et al., 2017). This latter coarse RCA fraction is the selected portion of starting material which undergoes the following investigations.

2.2. Methods

2.2.1. Preliminary image analysis assessment of attached mortar

Using a ZEISS stereomicroscope (SteREO Discovery V12) with an Axiocam 208 color camera mounting a fixed light source (CL 6000 LED) and a magnification of x10, digital images for more than 300 unique coarse RAs are acquired, being the most far-magnification feasible also by using high-resolution RGB camera. Following a first visual evaluation of the database, the population exhibits several forms of RAs (Fig. 1) within clean aggregates, intermediate mortar-covered aggregates, and full mortar-based aggregates.

The RAs samples images collected are subjected to IAM using ImageJ Software (Schneider et al., 2012) following the method proposed by Wang et al., 2021b. Each sample's image was analyzed to yield an estimation of the surface covered (SC %) from the attached mortar (for the entire collection of RAs images see Supplementary Materials). The initial stage of processing involves converting the RGB images to 8-bit grayscale, where each pixel is encoded using a grey scale from 0 to 255 (256 values), where 0 is black and 255 is white. ImageJ software allows to easily perform the 8-bit greyscale transformation of the starting database and also to define the correct scaling of the pixel/size ratio which has been fixed at 0.4 mm/pixel for the present application, same used in the cited work. The grayscale values, after Wang et al., 2021b, can be divided into three intervals, namely, 0–50, 50–175, and 175–255, respectively, corresponding to the pixel values of background, aggregates, and adhered mortar (Fig. 2).

The process of IAM can be divided into three steps: (I) image segmentation transformation, (II) filtering and denoising, and (III) boundary treatment. Segmentation is then conducted with a first cutoff threshold of 160, resulting in the individual RAs total area without the background. Furthermore, a consequent cutoff of 210 is applied to achieve a segmentation of the surface covered by AM. It is, afterwards, necessary to filter and denoise the greyscale image to remove impurity information in each region related to aggregate and adhered mortar after the segmental transformation of the grayscale image. Non-linear and component filters, such as median and opening filtering were used to deal with the grayscale image of RAs (Fig. 3). For an extended discussion of boundary treatment procedure and accuracy and precision of the used IAM see Wang et al., 2021b.

The quantitative information concerning 2D area is derived from pixel counting following the threshold of the 8-bit greyscale pictures. ImageJ's inbuilt tool "Analyze Particles" was used to carry out the measurements. Only regions larger than 1 mm^2 are tallied, and the minimum Area Size identified ($pixel^2$) is fixed at 50. Total Area (mm^2) is connected to the background's segmented surface, producing a figure for the bidimensional total area for each RAs. Instead, the value of Area Covered (mm^2) results from the pixel count coming from the latter segmentation at 210, which is tied to the associated mortar. The parameter of Surface Covered percentage (SC %) is then calculated using (1):

$$SC\ \% = \frac{Area\ Covered\ (mm^2)}{Total\ Area\ (mm^2)}*100 \tag{1}$$

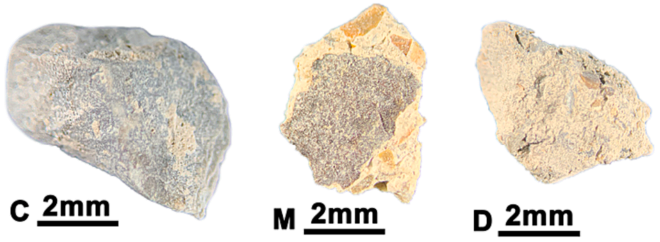

Fig. 1. Image taken with a high-resolution RGB camera of three distinct RAs samples., where C means clean aggregate, M stays for mortar covered aggregate and D for mortar-based aggregate.

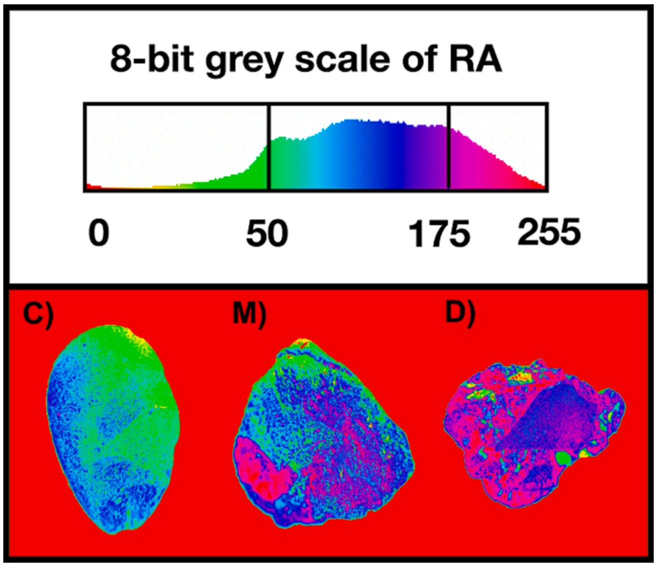

Fig. 2. Spectrum of 8-bit colored greyscale intensity of three RAs with different amount of AM on the surface (here again C stands for clean, M for mortar-covered and D for mortar-based aggregates).

2.2.2. Gaussian mixture model clustering of samples

Exploratory clustering analysis is used to determine the presence of subgroups of samples within the results obtained after the IAM (Section 2.2.1). The outputs of the IAM's Surface Covered Percentage (SC%) serves as a distinctive attribute for every single specimen in performing the analysis. Consequently, the initial RAs samples are divided into three distinct categories based on comparable AM content levels. The method of clustering chosen is the Gaussian Mixture Model (GMM), a parametric probability density function represented as a weighted sum of Gaussian component densities. GMM parameters are estimated with the iterative expectation–maximization (EM) algorithm using the Bayesian Information Criterion (BIC) for model selection (Yang et al., 2012). By employing BIC, we first establish K, which represents the total amount of Gaussian mixture components (Baudry et al., 2010). As a result, the best predicted model is displayed after a series of iterations. To explore the database, a starting model with two K components and full covariance is defined. In the end, clusters from the entirety of the population are fitted by independent Gaussian distributions.

2.2.3. Separation and quantification of AM by mechanical treatments

The groups of samples resulting from GMM clustering (Section 2.2.2) were individually processed to precisely quantify AM average percentage in the bulk material within 10 RAs. The experimental method followed the protocol by Tam et al., 2021, involving mechanical treatments like impact and abrasion to remove AM layers from clast surfaces and determine the average AM mass ratio (AM wt.%). An autogenous cleaning technique was applied by placing RAs samples in a rotating mill drum loaded to 33% and revolved at 1400 RPM for 20 min. The AM powder detached was then sieved at 5 μm and weighed, referred to as AM detached (g). These values, in combination with the total mass of RAs before processing, RAs total mass (g), were used to calculate the mass fraction wt.% of AM as follows:

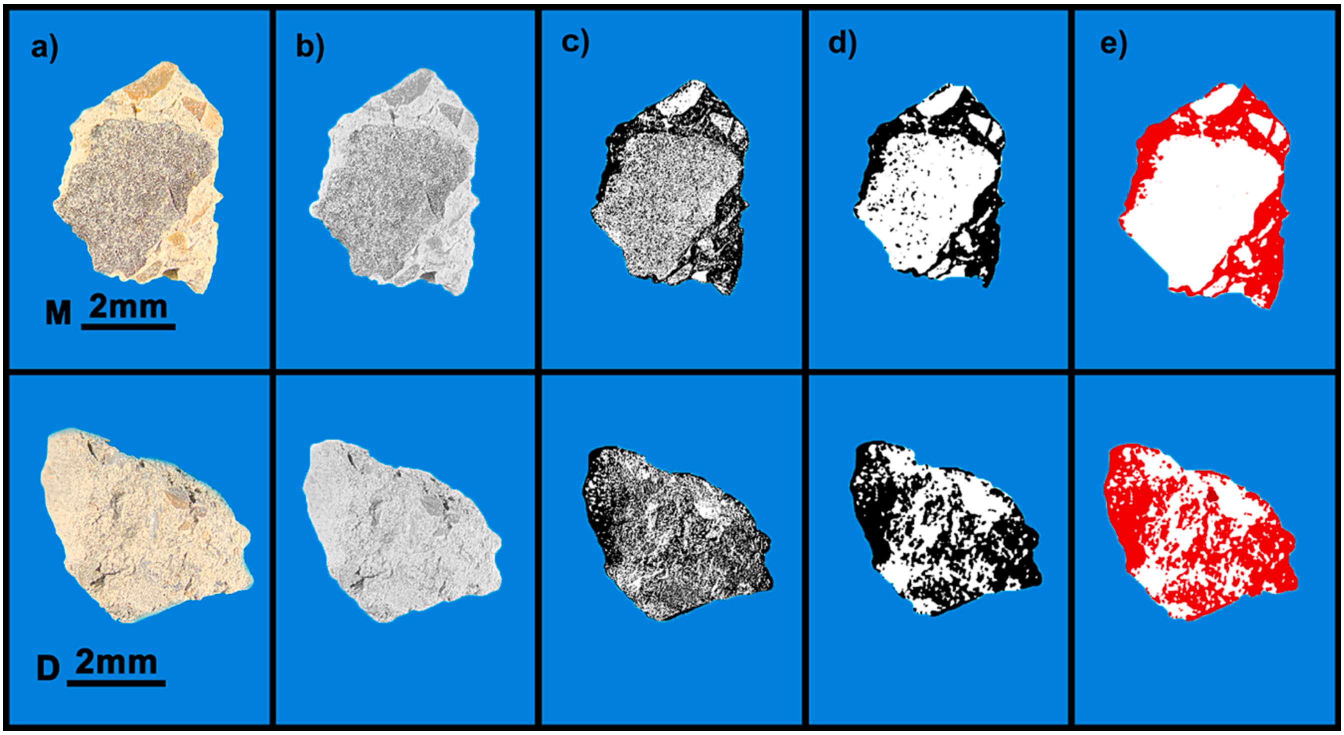

Fig. 3. Examples for M and D aggregates classes of the different IAM steps conducted: a) Original data (RGB), b) 8-bit transformed data (greyscale), c) Threshold for the 210 value, d) Filtering result, e) Pixel counted (Analyze Particle).

$$\text{AM mass ratio (wt.\%)} = \frac{\text{AM detached (g)}}{\text{RAs total mass (g)}} * 100 \tag{2}$$

2.2.4. *Computer-vision-based prediction of the attached mortar*

To achieve a more accurate and robust analysis, AI is employed to replace conventional image analysis for predicting the amount of mortar attached to recycled aggregate particles. Herein, a deep learning model (convolutional neural network, CNN) is trained to infer the mass fraction of the attached mortar, based on the same image of individual aggregate particles that is obtained from Sec. 2.2.1. The CNN approach is selected because it is well-recognized for visual imagery with its dominant superiority in accuracy and efficiency among all computer vision methods (Szeliski, 2022). Following the common practice, 80% of the images are used (i.e., training set) to train the model, while the remaining 20% of

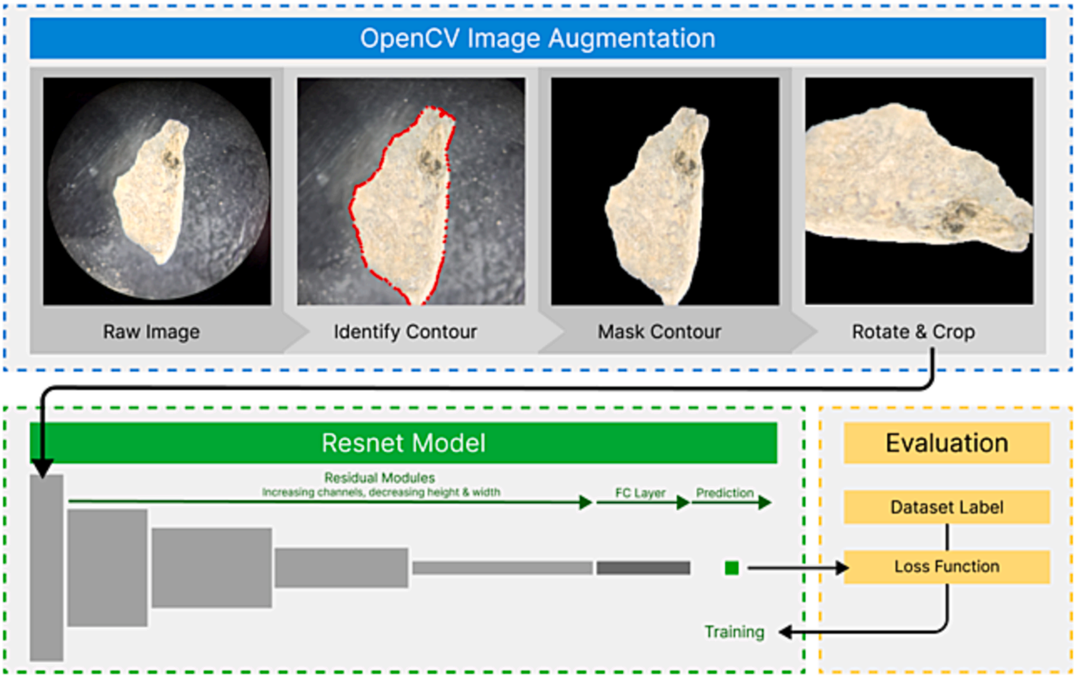

Fig. 4. Illustration of the pipeline for training the AI model. During training, the model is regularized for good generalizability such that it can predict the mass fraction of the attached mortar for new aggregate images that are not involved in the model training.

images (i.e., test set) are kept hidden for testing the prediction accuracy of the trained model. To avoid the bias related to randomness, it is adopted a stratified sampling for splitting the training and testing images (Song et al., 2020).

The pipeline of the AI analysis is illustrated in Fig. 4, and all the relevant data processing and modeling work are programmed in Python. Prior to the model training, the raw aggregate image is pre-processed to mask the non-aggregate region. This step removes irrelevant information associated with the background, which essentially ensures that the model only learns to make predictions based on aggregate-related data. Otherwise, the model could fit irrelevant features appearing in the background. The background removal is done by filtering the raw image based on brightness, using basic functions in the OpenCV package an open-source computer vision library (Bradski, 2000).

The model training is driven by minimizing the mean squared error (MSE) loss between the predicted and true mass fractions of the attached mortar, with careful consideration of several settings. In order to facilitate a consistent learning process, a small learning rate of 0.0001 was adopted. This choice aimed to ensure gradual updates and prevent abrupt changes that may hinder convergence. Additionally, a weight decay of 0.0001 is implemented to effectively regulate the model's learning process and prevent overfitting on the training data. To sufficiently capture the underlying patterns and optimize the model's performance, the training was conducted over a total of 100 epochs, allowing for extensive iteration and refinement. To further improve the stability of the model prediction, the model training is repeated five times so as to obtain five individual models. Thus, the final prediction for a given input is based on the ensembled predictions yielded from the five individual models, by taking the average. The model predictions presented in the following sections are all based on the ensemble prediction.

A common challenge faced by material studies lies in training machine learning models with a small number of samples (e.g., less than tens of thousands of images). This issue also applies to the present study, as the limited size of the aggregate image dataset does not allow training a deep learning model from scratch. To overcome this issue, special attention is paid to addressing this issue. First, the ResNet-18 is adopted as the backbone model (He et al., 2015). In comparison to other deep learning models that usually have much deeper and more complex networks, ResNet-18 is selected because it is relatively simple, and requires less data to achieve decent training outcomes. In addition to ResNet-18, the model is trained based on the pretrained model parameters from IMAGENET1k (Russakovsky et al., 2015). This approach, also known as transfer learning, is a popular technique in the field of computer vision for training deep learning models based on small datasets. The idea of transfer learning is that, while the pretrained model parameters are originally optimized for other visual analysis tasks (e.g., recognizing different animals), some of them are generic for detecting shapes or patterns so that adopting the pretrained model parameters allows the new model to learn the task-specific features more effectively from the new dataset. To enable the use of the original ResNet-18 model for the purposes of this study, the structure is slightly modified. Instead of a one-hot output with the original size 1000 associated with IMAGENET1k, our model uses three fully connected layers with sizes of 8, 4, and 1, with Rectified Linear Unit (ReLU) and batch normalization layers between each two. This allows our model to output a single value that represents the prediction for the mass fraction of the attached mortar. Given the small learning rate adopted for model training (0.0001), the transferred model is not frozen during retraining. Furthermore, during model training, the training images are augmented with image jittering (e.g., random rotation, flipping, etc.). Doing so allows an improved data variation, which contributes to enhancing the model robustness with a fixed number of training images. Readers seeking additional explanations on CNN, transfer learning, and image augmentation are referred to a previous publication (Song et al., 2020).

2.2.5. *X-ray powder diffraction analysis and Rietveld refinement*

The powder of AM obtained from each group resulting from mechanical detaching (Section 2.2.3) is further analyzed using X-ray powder diffraction technique (XRPD). The XRPD patterns are collected at room temperature in the 2θ range of 5-90° using a Bruker D8 Advance Da Vinci diffractometer. Phase identification is carried out with DIFFRACT.EVA suite utilizing the Powder Diffraction File (PDF-2) database maintained by the International Centre for Diffraction Data (ICDD). An accurate quantitative phase analysis (QPA) is performed using the Rietveld profile fitting method applied to the X-ray diffraction patterns, using the Bruker TOPAS 5.0 software. In order to reduce discrepancies between a computed profile and the measured powder diffraction profile, the whole-profile Rietveld method employs a least squares minimization strategy. The Rietveld technique is developed to determine quantitative information of complex mixtures of crystalline phases using laboratory X-ray diffractometers. The weight percentages (wt. %) of each crystalline phase detected from XRPD are determined after performing the aforementioned Rietveld refining. The reader might look to a more specialized literature for an expanded discussion of the Rietveld refinement procedure. (Aranda et al., 2012; Le Saoût et al., 2011).

2.2.6. *Rietveld based reconstruction of attached mortar*

Following XRPD, the reconstruction of AM volume and carbonation degree for every group of samples is performed from a novel mineralogical model introduced. Weight percentages of crystalline minerals resulting from Rietveld QPA provide essential "fingerprint" data for the average mineral composition across multiple samples, as described in Sections 2.2.1 & 2.2.2. The model incorporates the weight percentages of identified crystalline phases ($\mathrm{Wt}_{(i)}$), normalized to unity, and uses tabulated densities (g/mm^3) from literature for silicates, carbonates, and synthetic cement product phases (Balonis & Glasser, 2009) as parameters in Eq. (3). Each parameter is a weighted mean based on the QPA-Rietveld percentages. Subsequently, the ratio of AM mass (g) measured after the detachment procedure is introduced to estimate AM Volume coverage in mm^3, as described in Eq. (5).

$$AM\ Volume\ \left(mm^3\right) = \frac{AM\ (g)}{\left(\sum_{i=1}^{n} Wt_{(i)} {}^{*} \rho_{tab}\right)/N} \tag{3}$$

Where AM is the mass of powder obtained from each group, ρ_{tab} is the tabulated density of mineral (i), *Wt* is value from 0 to 1 from wt.% of mineral (i) from QPA-Rietveld.

The volume (%) of attached mortar in RAs groups can be obtained by combining AM Volume (mm^3) data from QPA-Rietveld with IAM results (Section 2.2.1). Despite some deviations from the theoretical description, the presence of 10 individual RA exemplars in each group corrects the overall data, yielding average values for Total Area in mm^2 (1) used to calculate the sample average radius from (4):

$$RA\ radius = \sqrt{\frac{Total\ Area\ \left(mm^2\right)}{4\pi}} \tag{4}$$

and then a measurement of the volume is easily obtained with (5):

$$RA\ volume = \left(\frac{4}{3}\right)\pi\ {}^{*}\ (RA\ radius)^3 \tag{5}$$

The final volume (%) of attached mortar which covers the RAs surface (3DC%) is then obtained as (6):

$$3DC\ \% = \frac{AM\ volume\ \left(mm^3\right)}{RAs\ volume\ \left(mm^3\right)} {}^{*}100 \tag{6}$$

In conclusion the final database (See Section 3.4 and Supplementary Materials) consists for each group of a calculated average total volume of the RAs (mm^3) resulting from combined IAM and QPA-Rietveld.

3. Results and discussion

3.1. ImageJ analysis and GMM clustering

Following the IAM method, the starting dataset of 300 RAs is divided into three subgroups (for the individual values of SC% see Supplementary Materials), primarily as a result of the GMM clustering procedure used (Fig. 5). The quantile–quantile plot (Q-Q plot) in Fig. 6 shows a linear trend by dispersing the quantile distribution among the beginning data with the predicted mixture distribution reflecting the model's effectiveness in fitting after 10,000 iterations. Following the first IAM quantitative analysis, a first batch of 100 individual samples provided SC% values of 0. As a result, they were categorized as clean RAs (C-RA) and aren't shown in plots. Following that, the GMM model's implementation produced a first Normal Distribution that described a population of unique RAs with a mean value of 47 SC% that were ascribed to the M−RA group. The model simultaneously fits a second Normal Distribution with a mean of 67 SC% allowing to classify these data as D-RA.

Eventually, the initial RAs samples are separated into three groups called C-RA, M−RA, and D-RA based on comparable AM content levels. In order to group 300 individual RAs-analyzed samples into 30 groups with similar SC% values, 10 singular clasts were used (Fig. 7). In total, there are ten groups in each of the three major categories (C from 1 to 10, M from 1 to 10, and D from 1 to 10). The division of the RAs into three distinct macro-groups (C, M, and D) is consistent with earlier research (Kim, 2022; Liu et al., 2022; Mazhoud et al., 2022) within: mortar-free RAs (C-RA) being similar to natural aggregates, mortar-covered RAs (M−RA) which only has partial areas of surface AM, and mortar-based RAs (D-RA) which is primarily comparable to pure hydrated cement paste.

3.2. Detaching AM by mechanical treatment

Following the mechanical treatment based on rotational milling and sieving tests the following values are obtained for the sub-groups composed of 10 individual RAs merged from the IAM and GMM clustering technique (Table 1 and complete set on Supplementary materials). The powder amount mechanically detached and collected from each group represents an accurate measurement of average AM content, presented as AM mass ratio (%). The results obtained for the samples belonging to the C-RA category mainly confirm the IAM procedure's findings that AM is not present in C-RA groups. In fact, no powder was found within the aforementioned specimens following the detaching procedure. After the same treatment, the M−RA category displaying an intermediate AM content exhibiting an average RAs total mass of 7.11 g and of 0.25 g of pure AM, which is equivalent to a mean AM mass ratio of 3.51 wt%. Finally, for the D-RA category, which according to GMM has the greatest AM content, an average total mass of 5.31 g and of 0.54 g of pure AM is reported, which is equivalent to a mean percentage of detached powder of 10.11 wt%. The average density of the surface layer of the AM is 1.8–2.2 g/cm^3 due to the high inherent porosity of the dried cement paste, whereas the value for the natural mineral pieces of aggregates embedded is around 2.8–3.0 g/cm^3 (Bai et al., 2020; Xiao et al., 2006).

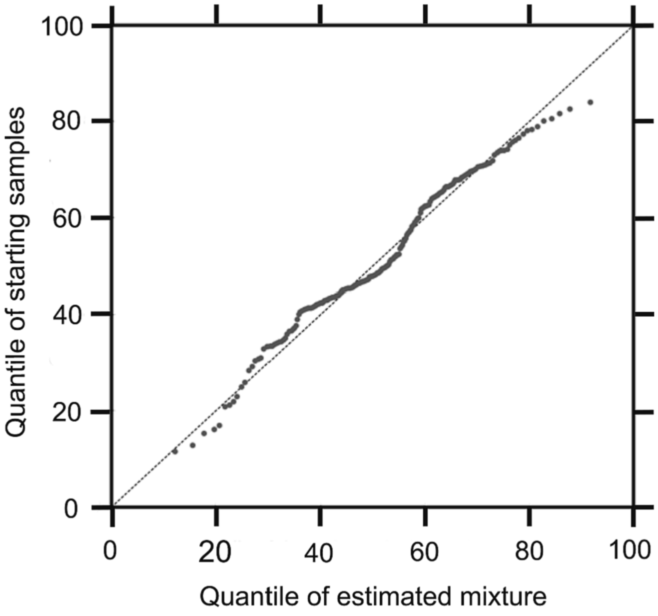

Fig. 6. Q-Q plot of the quantiles from original samples vs the estimated mixture distribution.

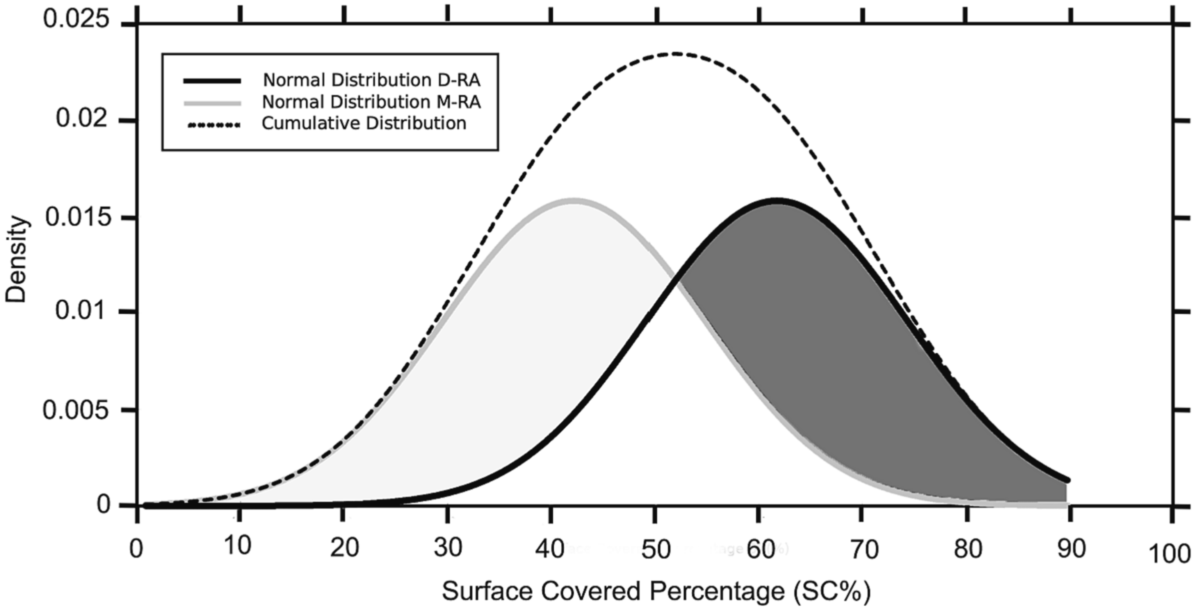

Fig. 5. Gaussian Mixture Model clustering of samples, dark line defines the Normal Distribution for D-RA and light line defines the Normal Distribution for M−RA, dotted line stands for the Cumulative Distribution calculated.

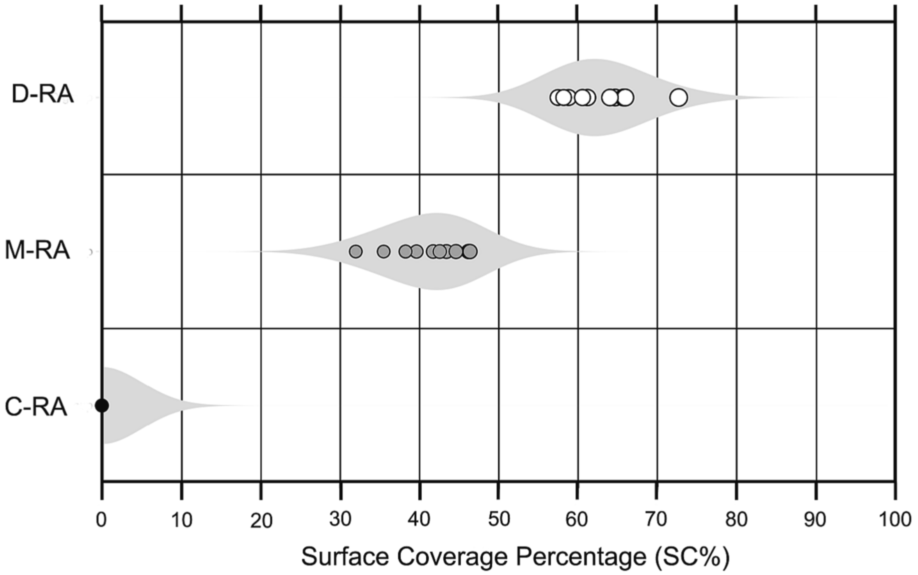

Fig. 7. Violin plot distribution of the 30 groups resulting from the GMM divided into C-MA, M−RA and D-RA.

Table 1
Results of Mechanical Treatments conducted on M−RA and D-RA.

Sub-Group (from 1 to 10)	Average RA Tot. mass (g)	Average AM mass (g)	Average NA Weight (g)	Average AM mass ratio (%)
C-RA	5.63	0	5.63	0
M−RA	7.11	0.25	6.86	3.51
D-RA	5.31	0.54	4.77	10.47

3.3. XRPD powder analysis and QPA-Rietveld

The XRPD pattern collected involved the subgroup M−RA and D-RA, being in total composed of 20 distinct samples of AM powders removed after the mechanical treatment among 10 individual RAs within each group. The occurence of residual cement minerals and other secondary crystalline phases is indentified from peak positions (vaterite, aragonite, ettringite, AFm phases, namely the calcium aluminate ferrite hydrates both tri- and mono-substituted) which represent the hydration and carbonatation products of the cement paste. The occurrence of feldspars and quartz likely stands for micro-aggregates powder embedded inside the AM. The presence of calcite can be present either as micro-aggregate (primary), or more important as a main carbonatation product (secondary) together with vaterite and aragonite. The occurrence of both primary and secondary calcite is revealed by the asymmetry of the main peak of calcite (at 29.6° 2θ) which was modeled using two types of calcites with different crystallite sizes: a type-1 calcite with an average crystallite size of 80 nm and a type-2 calcite with a value of 25 nm (Fig. 8). The formation of bimodal crystallite size of calcite (the secondary with 25 nm), and of the $CaCO_3$ polymorphs (vaterite and aragonite), can be due to different cement type used, CO_2 partial pressure, or the carbonatation of different hydrated products, namely C-S-H, ettringite, or AFm (Auroy et al., 2018; Goñi et al., 2002; Y. Li et al., 2020). The anhydrous cement phases (C3S, C2S, C4AF, C3A) represent unreacted crustal of cement paste, which are always found together with the hydration product inside the matrix. Following QPA-Rietveld each identified mineralogical phase is quantified (wt. %) in every sample analyzed (see Supplementary Materials for the complete list).

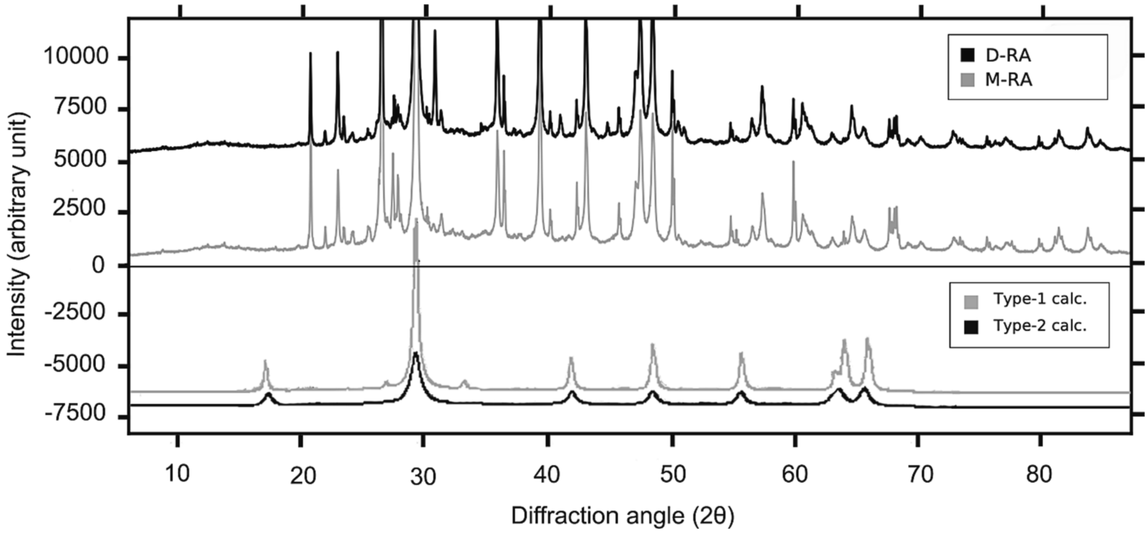

Fig. 8. XRPD pattern of D-RA compared to M−RA and bimodal crystallite site of two types of calcites identified.

3.4. QPA-rietveld based model reconstruction of attached mortar and carbonation degree

To generate a mineralogical model and to obtain the volumetric crystalline assemblage (mm^3) of the studied AM powders, bulk tabulated density parameters from mineralogical components discovered using XRPD are encompassed (the used values are provided in the Supplementary Materials). From the solutions of Eq. (3), AM volumes for M−RAs are determined to be around 50 and 125 mm^3, whereas AM volumes for D-RAs are found between 125 and 300 mm^3. Thus, the outcomes of Eq. (5)'s image analysis total volume reconstruction demonstrate that the mean total RAs volumes for M−RA and D-RA are 470 mm^3 and 418 mm^3, respectively. Ultimately, using Eq. (6), it is possible to obtain information that falls within a wide range of AM volume ratio (3DC%) values, enabling comparison of the extent of AM reconstructed from the model with the entire RAs volume calculated for each sample under consideration. The comparison of the 3DC% volume coverage with the AM mass ratio (wt. %) obtained for the same samples after mechanical detaching shows a good linear correlation ($R = 0.94$), and almost all the values are contained inside the standard deviation of the dataset (Fig. 9). This investigation demonstrates that the microscopical assemblage acquired from XRPD QPA-Rietveld may be utilized to rebuild the volume of AM covering the surface of RAs throughout a whole range of values (from 9 to 95%). A substantial boundary separation between the two GMM-generated subgroups is still there after charting the findings. A first compact cluster of scatter data related to M−RA exhibit an estimated volume coverage ratio ranging from 9% to 23%, while a second, more scattered group of samples associated to the D-RA ranges from 25% to 95%.

Furthermore, using the same model it was possible to determine and quantify the level of carbonation of the AM cement paste. From the QPA-Rietveld fitting model of the bimodal crystallite size of calcite (25 nm) and the $CaCO_3$ polymorphs (vaterite and aragonite) we obtained quantitative information on the wt.% of carbonation products for each sample. In Fig. 10, the results of computing the Carbonation volume ratio (CARB%) of the AM using the total sum of weights (%) of carbonation products after XRPD studies are shown. The values are obtained employing again the Eq. (6), based on the mineralogical model proposed in Eq. (3). The fraction of AM that is carbonated among the two subgroups is essentially uniform, having a mean value throughout the whole range of 20.61%. This can be explained by the homogenous source of waste stream taken as a sample in the present study. Instead, due to various aging, environmental circumstances during disposal, and the initial composition of the cement used, the carbonation level of the residual paste attached may vary substantially.

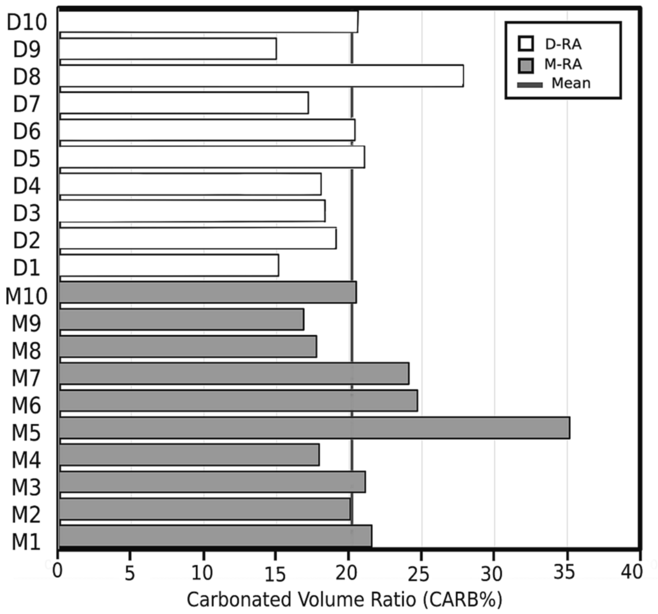

Fig. 10. Results of the estimation of the carbonation volume (%) of the attached mortar within the samples.

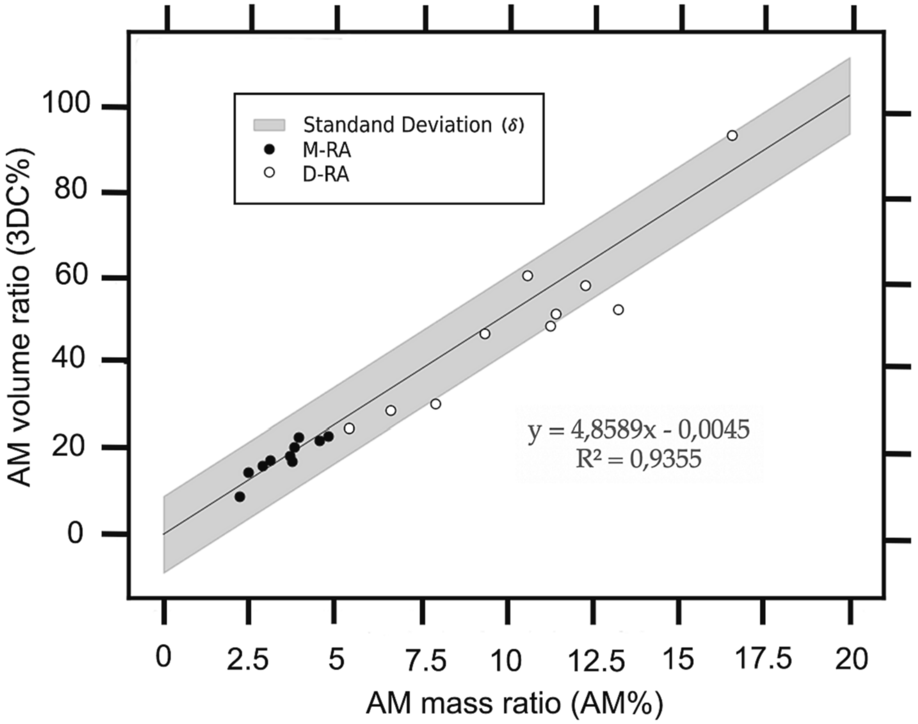

Fig. 9. Relation between calculated AM volume ratio (3DC%) obtained from a QPA-Rietveld based model and the values of AM mass ratio (AM%) from the mechanical detaching from the surface of RAs.

3.5. Computer-vision-based prediction of attached mortar

To enable a high-throughput classification of the recycled aggregate, a deep learning model is developed and trained to predict the mass fraction of the attached mortar based on the sole input of the photo of individual aggregate particles. In the context of our study, it is worth noting that, although predicting a 3D-based concept (i.e., mass fraction of the attached mortar) from 2D data (i.e., photo of the recycled aggregate) may not immediately appear intuitive. However, it is not uncommon for latent correlations to underlie the feasibility of such a 2D-to-3D mapping. Most likely, the aggregate samples of similar mortar attachments tend to exhibit comparable 2D appearances—for instance, an aggregate with even, brownish color is more likely to be coated with a thick layer of mortar than that showing a mix of different colors. Other examples include but are not limited to aggregate size, surface texture, and origin.

The model is trained using 80% of the images collected in this study (see Sec. 2.2.1). Upon completion of the model training, the accuracy of the model was tested based on the remaining 20% of images. This evaluation of the test set images offers insight into the model's effectiveness in predicting the AM of new aggregate samples that were not previously included in the model's training phase. In Fig. 11 is displayed the evolution of the model accuracy on both training and test sets over the 100 training epochs (i.e., 100 iterations of model training). As a common practice, the model accuracy in this plot is indicated by the mean squared error (MSE) loss, where lower loss means higher prediction accuracy. It can be seen that, as the training proceeds, the model loss decreases exponentially and plateaus at around 60 epochs. After that, model performance gradually converges to a steady stage where a small divergence between training and test sets is observed. This low level of overfit is deemed to be acceptable considering the limited size of the training dataset.

As an assessment of the model's performance after the training, Fig. 11 shows its predictions for both the training and test samples. Here, the presence of vertical patterns in the plot is attributed to the fact that, during the mechanical test (refer to Section 2.2.3), each of the ground truth values is obtained as the mass fraction averaged over the 10 samples of the same set. In terms of the model prediction for the training samples, we note that the scatters are distributed tightly along the line of equality, indicating that the model can fit the training samples well. At different levels of the mortar fraction along the x-axis, the predicted values vary within a certain range. In addition to the variation of the aggregate appearance, this is also related to the noise in the dataset, for example, it is difficult to obtain an ideal focus for the whole aggregate particle consistently for each sample under the stereological microscope. Nevertheless, with the sole input of the 2D aggregate image, it is encouraging that the model can yield fairly accurate predictions for most of the training samples, especially given that the prediction target depends on the aggregate volume in 3D.

Regarding the prediction for the test samples, the results indicate that the model can still yield reasonably accurate predictions, where the root mean square error (RMSE) on the test set samples is merely 2.8%. Regarding the model accuracy, Fig. 12 indicates that the model exhibits

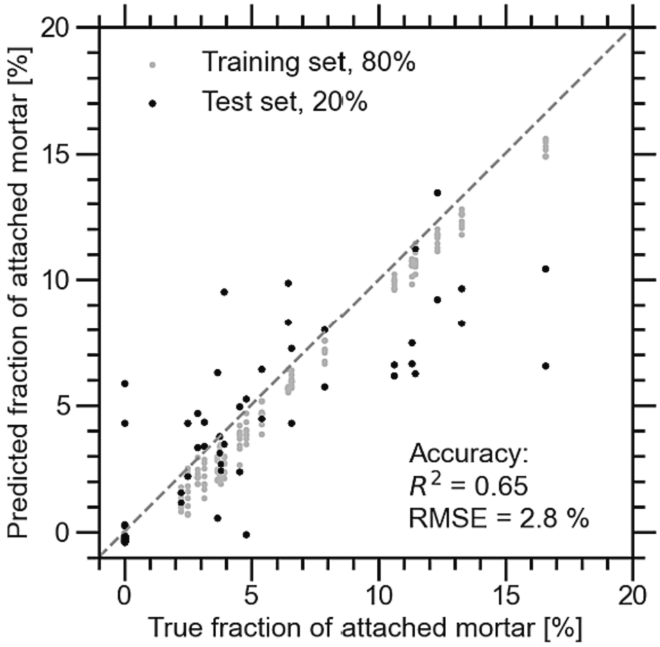

Fig. 12. Prediction of the mass fraction of the attached mortar for the different samples in the recycled aggregate dataset. The blue scatters correspond to the 80% samples in the training set and the 20% samples in the test set, respectively.

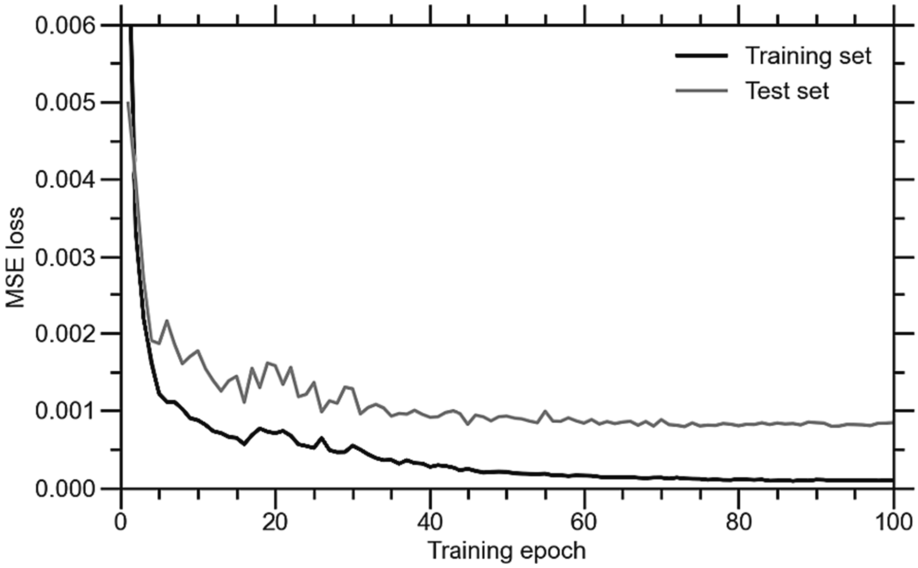

Fig. 11. Evolution of mean squared error (MSE) loss of the model with the increase of training epoch, based on both training and test sets. The model loss here indicates the improvement of the model accuracy as a function of the training iterations.

fairly high accuracy on the samples within the C-RA and M−RA groups, as well as most of the samples in the D-RA group up to about 10%. To assess the model's robustness more comprehensively, we present the distribution of prediction errors (i.e., predictions minus true values) for the test set samples in Fig. 13. The analysis reveals that the distribution of the prediction errors is roughly symmetric, with approximately 40% of the test samples falling within a deviation of ± 1%. This observation indicates no significant bias in the model's predictions on the test set, underscoring the robustness of its predictive capabilities.

From Fig. 12, it can be also seen that the predicted values are somewhat capped at about 10%, indicating that the model does not generalize well for aggregates that are heavily coated with the mortar. This should be attributed to the fact that there are limited samples with very high fractions of the attached mortar within the present dataset. Thus, the model is not sufficiently trained to extrapolate beyond the aggregates containing more than 10% of the attached mortar. In addition, it is also possible that aggregates appear very similar after reaching a certain fraction of attached mortar (such as color tone and surface texture). In such a case, it becomes intrinsically challenging to predict the samples of very high AM% regardless of processing methods.

3.6. Empowering the high-throughput screening of recycled aggregates with artificial intelligence

Based on the results presented in Sec. 3.6, we now discuss the potential of using our deep learning model to enable the high-throughput classification of recycled aggregates. We first note that the trained model exhibits fairly accurate predictions on the recycled aggregate dataset curated in this study. This is not only observed from the samples used for training the model, but also for most of the test set samples that are never involved with the model training. To this end, the results presented in Fig. 9 are further analyzed to obtain a confusion matrix to reflect the model performance in differentiating the three classes of recycled aggregates with different AM amounts—namely, Low: <2%, Medium: 2-to-5.1%, and High: >5.1%, as shown in Table 2. Note that, to obtain a fair assessment of the model accuracy on predicting samples that are not seen during training, all the results presented in Table 2 are solely based on the test set samples and intersection over union (IoU) is considered as the metric for classification accuracy.

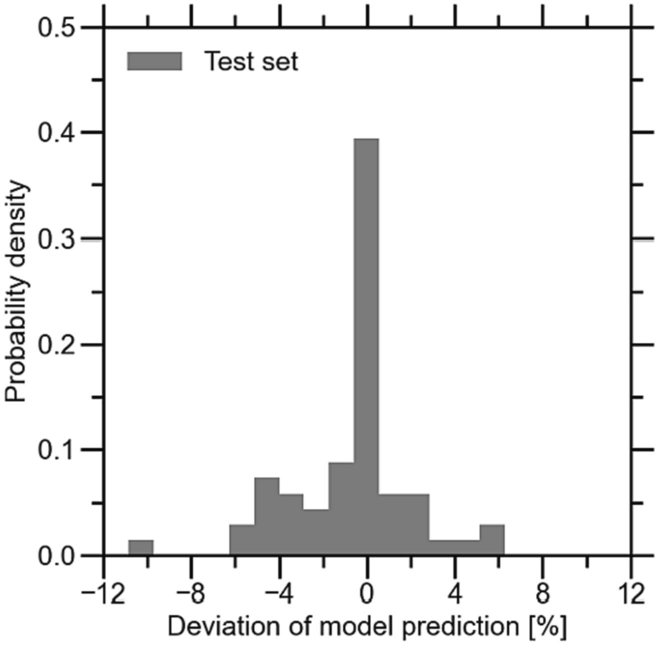

Fig. 13. Distribution of the prediction error for the test set samples. Here, the deviation of model prediction is defined as the difference in the mass fraction of the attached mortar (i.e., prediction – true).

Table 2
Confusion matrix of the deep learning model for classifying the recycled aggregate samples in the test set (i.e., 20% of the samples at each AM% level), along with the intersection over union (IoU) accuracy.

Confusion matrix		Predicted AM%			IoU accuracy [%]
		C-RA	M−RA	D-RA	
True AM%	Low (<2.0%)	18	1	1	75
	Medium (2.0–5.1%)	4	13	3	57
	High (>5.1%)	0	2	18	75

Considering the noise in the dataset and the intrinsic difficulty in inferring the mass fraction of the attached mortar based on 2D images, the deep learning model offers a desirable classification accuracy. In comparison, the model performs best in detecting the C-RA and D-RA, where only 2 out of 20 samples in both of those groups are misclassified. Furthermore, no aggregate from the D-RA group is misclassified into the C-RA group. In comparison, the model exhibits inferior accuracy in recognizing the samples in the M−RA group. With the IoU accuracy almost 20% lower than the other two classes, 20% and 15% of the M−RA samples are predicted to be C-RA and D-RA, respectively. This can be attributed to two reasons. Firstly, the averaged AM% values for each set of samples may not accurately capture the variation of attached mortar in the individual samples under each set. Secondly, the variation in model predictions leads to confusion due to the gradual transition in appearance between C-RA, M−RA, and D-RA, which is exacerbated by the much smaller band of values occupied by the category.

Despite the above-mentioned challenges faced by the model prediction, we highlight several significant advantages of our proposed computer-vision-based model in addressing the critical requirement for rapid classification in high throughput screening of recycled aggregates.

1. By leveraging the deep learning, we are able to provide instantaneous predictions of the AM% for a given aggregate image. Notably, as a regression model, it demonstrates commendable accuracy, yielding reliable inferences of the AM mass ratio (%) within a range of up to 10%.
2. Meanwhile, when converting the predicted values into aggregate classes, our model exhibits an impressive 90% recall rate in accurately predicting the C-RA and D-RA aggregate categories.
3. An additional strength lies in the fully automatic training process of the deep learning model, eliminating the need for manual judgments such as determining color thresholds for specific image datasets.

3.7. Enhancing RAs recycling by deep learning and mineralogical models

In addition to classifying the waste according to the predicted AM fraction using deep learning, another step is done to increase the likelihood of recycling and reusing C&DW in new construction materials. While determining the best strategies to recover C&DW from old concrete, the AM content is not the only factor to consider.

1. The mineralogical composition of the AM can vary abundantly, being primarily affected by the degree of carbonation of the layer itself due to various aging, environmental circumstances during disposal, and the initial composition of the cement used. The final result is a variety of raw material byproducts with various chemical and physical characteristics, depending on the degree of carbonation.
2. After using the QPA-Rietveld mineralogical model and utilizing the methodological technique based on GMM clustering of samples and mechanical detachment of AM, the best suited methods to reuse the C&DW can be established in customized application. This step could

represent the final stage of a decision-making process in terms of choosing a technological and organizational solution in the field of concrete waste management (Sobotka & Sagan, 2021). This data structure can be combined and integrated with actual project workflows, including time, cost, and other supply chain indicators that aid in informed decision-making (Sivashanmugam et al., 2023).

3. If the optimum way to reuse C-RA is always to employ them as brand-new aggregates in fresh concrete, suggesting a similar procedure for M−RA and D-RA could be not advantageous. The two parameters that needs to be taken into account simultaneously are the AM content and the carbonation degree of the connected residual cement paste (Fig. 14).
4. The materials classified as M−RA can be categorized as natural aggregates with less than 25% volume ratio of cement paste connected (Fig. 9), and the reuse as RAs can be determined depending on the AM’s degree of carbonation. If the materials present a low-carbonation of the AM the best solution is to reuse them as RAs after removing mechanically, chemically or thermally the old interfacial transition zone layer (Ouyang et al., 2020; R. Wang et al., 2020). Instead, a positive interaction forms when the components are utilized inside fresh cement paste if the AM layer has a high carbonation degree (Stefaniuk et al., 2023). The carbonation process led to the formation of silica gel which transforms the materials in a pozzolanic source, giving to the new cement matrix a recovery of latent performances of the available cement phases (Lu et al., 2019; R. Wang et al., 2020).
5. The D-RA class display a volume of AM that is never suitable for use as new aggregates in concrete, superior to 25% volume ratio (Fig. 9). Once more, if the materials exhibit a modest degree of carbonation, they can be used as by-products of raw-mix materials for the clinker production since they are a good supply of carbonate and silico aluminate to be used in the kiln (De Schepper et al., 2013). Instead, if they exhibit a high carbonation level, they once more constitute a reliable supply of pozzolanic materials and can be then included as supplemental cementitious materials in a mixture with new clinker (Moreno-Juez et al., 2021;Stefaniuk et al., 2023).

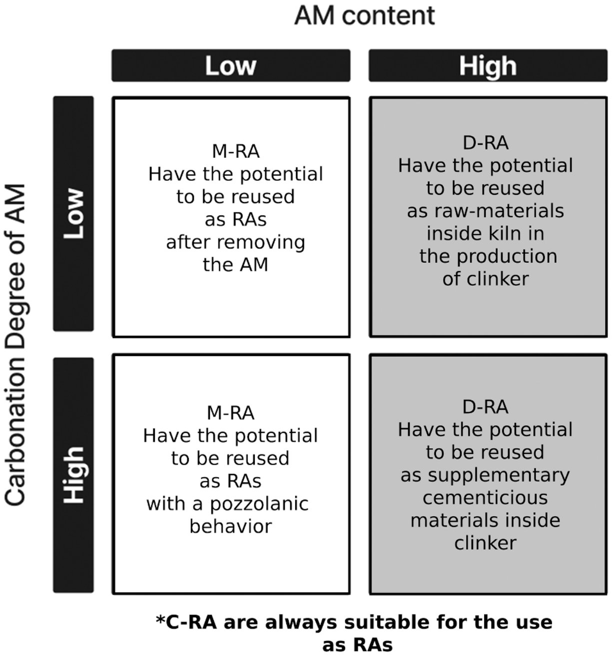

Fig. 14. Schematic description for the best suited methods to reuse the C&DW can be established in customized application.

4. Conclusions

The approach based on IAM, machine learning and mineralogical laboratory methods to determine the residual attached mortar volume and to estimate the carbonation degree led to the following conclusions:

1. Although the use of IAM to estimate the amount of AM on the surface of RAs seems to be a trustworthy way to quantify the AM content, it is nevertheless susceptible to inaccuracies from human sources. The improvement made from the computer-vision-based model gives less uncertainty and higher accuracy in predicting the AM content on surface of RAs.
2. By leveraging the deep learning, we are able to provide instantaneous qualitative predictions of the AM content for a given aggregate image. Notably, as a regression model, it demonstrates commendable accuracy, yielding reliable inferences of the AM mass ratio (%) within a short range of values.
3. Our model shows an impressive 90% recall rate in correctly predicting the C-RA materials and D-RA aggregate categories when converting the predicted values into aggregate classes. This result shows that a portion of high-quality secondary raw materials (C-RA) can be extracted from the C&DW unsorted waste stream using an optical-based sorting plant that employs artificial intelligence. These RAs can be fully reused in the production of concrete without compromising the overall engineering properties due to the presence of residual AM, making them perfectly comparable to those derived from nature’s resources.
4. The mineralogical model introduced to reconstruct the volume of attached mortar paste on the surface of RAs from XRPD and Rietveld refinement displayed a strong correlation (R^2 0.94) with the measured attached mortar mass, representing a valid and viable method to estimate this parameter.
5. By using the same model, it is possible to obtain an indication of the degree of carbonation of the connected residual cement paste. Even though this data is less precise and sensitive than other known analytical technique and methods currently available, it may nevertheless be more usefully utilized for a fast evaluation and categorization of the secondary materials.
6. Different potential final uses for the C&DW are discussed, depending on the AM concentration and cement paste carbonation level, it is not possible to rely solely on one of them in order to achieve the effective reuse of these materials. Because both of these factors are significant to define tailored reuse of RAs, toward the sustainable development of the building material sector.

It is worth mentioning that despite more testing is required to better calibrate the procedure with industrial operating conditions, such as high fluxes of simultaneous materials to be analyzed, dry and wet conditions and RGB camera settings, the technology proposed has the potential to be scaled in large-scale optical sorting plants for C&DW. It is essential to validate all these results in the real-world application.

The future objective of this research is to establish an extensive laboratory characterization of AM on C&DW sorted materials for verifying the accuracy of the prediction’s outcomes, as well as to conduct continuous test on the reuse of these secondary raw-materials in different building materials applications based on the mineralogical method proposed.

CRediT authorship contribution statement

Andrea Bisciotti: Conceptualization, Methodology, Formal analysis, Investigation, Data curation, Writing – original draft, Visualization. **Derek Jiang:** Investigation, Software, Validation. **Yu Song:** Methodology, Validation, Formal analysis, Writing – original draft, Supervision. **Giuseppe Cruciani:** Validation, Resources, Writing – review & editing, Supervision, Funding acquisition.

Declaration of competing interest

The authors declare that they have no known competing financial interests or personal relationships that could have appeared to influence the work reported in this paper.

Data availability

Data will be made available on request.

Acknowledgments

We would like to express our sincere thanks to Fabio Pelliccia of Pelliccia Scavi Srl for kindly providing the materials under study. We would also like to thank Tereza Fantová from the University of Ostrava for proofreading the work.

Funding

The project was founded by the grant 2018_DE_MIUR_FST_DOOR_sede_BA—BORSA DOTTORATO XXXVII CICLO – Bisciotti Andrea (Quota attività di ricerca) as part of the financial assistance for "Departments of Excellence" by the Law 232 of 2016.

Appendix A. Supplementary data

Supplementary data to this article can be found online at https://doi.org/10.1016/j.clema.2023.100215.

References

Abbas, A., Fathifazl, G., Fournier, B., Isgor, O.B., Zavadil, R., Razaqpur, A.G., Foo, S., 2009. Quantification of the residual mortar content in recycled concrete aggregates by image analysis. Mater Charact 60 (7), 716–728. https://doi.org/10.1016/j.matchar.2009.01.010.

Abzaev, Y., Gnyrya, A., Korobkov, S., Gauss, K., Boyarintsev, A., Tomrachev, S., 2019. Thermodynamic modeling of Portland cement without mineral additives. J. Phys. Conf. Ser. 1145 (1) https://doi.org/10.1088/1742-6596/1145/1/012016.

Aranda, M.A.G., De La Torre, Á.G., León-Reina, L., 2012. Rietveld quantitative phase analysis of OPC clinkers, cements and hydration products. In. Rev. Mineral. Geochem. 74, 169–209. https://doi.org/10.2138/rmg.2012.74.5.

Auroy, M., Poyet, S., Le Bescop, P., Torrenti, J.M., Charpentier, T., Moskura, M., Bourbon, X., 2018. Comparison between natural and accelerated carbonation (3% CO2): Impact on mineralogy, microstructure, water retention and cracking. Cem. Concr. Res. 109, 64–80. https://doi.org/10.1016/j.cemconres.2018.04.012.

Bai, G., Zhu, C., Liu, C., Liu, B., 2020. An evaluation of the recycled aggregate characteristics and the recycled aggregate concrete mechanical properties. In: Construction and Building Materials, Vol. 240. Elsevier Ltd. https://doi.org/10.1016/j.conbuildmat.2019.117978

Balonis, M., & Glasser, F. P. (2009). The density of cement phases. In *Cement and Concrete Research* (Vol. 39, Issue 9, pp. 733–739). https://doi.org/10.1016/j.cemconres.2009.06.005.

Baudry, J.P., Raftery, A.E., Celeux, G., Lo, K., Gottardo, R., 2010. Combining mixture components for clustering. J. Comput. Graph. Stat. 19 (2), 332–353. https://doi.org/10.1198/jcgs.2010.08111.

Bonifazi, G., Palmieri, R., Serranti, S., 2018. Evaluation of attached mortar on recycled concrete aggregates by hyperspectral imaging. Constr. Build. Mater. 169, 835–842. https://doi.org/10.1016/j.conbuildmat.2018.03.048.

Bradski, G., 2000. The OpenCV Library. Dr. Dobb's J. Software Tools.

Braymand, S., Roux, S., Fares, H., Déodonne, K., Feugeas, F., 2017. Separation and quantification of attached mortar in recycled concrete aggregates. Waste Biomass Valoriz. 8 (5), 1393–1407. https://doi.org/10.1007/s12649-016-9771-2.

Das, A., Song, Y., Mantellato, S., Wangler, T., Lange, D.A., Flatt, R.J., 2022. Effect of processing on the air void system of 3D printed concrete. Cem. Concr. Res. 156, 106789 https://doi.org/10.1016/j.cemconres.2022.106789.

De Schepper, M., De Buysser, K., Van Driessche, I., De Belie, N., 2013. The regeneration of cement out of Completely Recyclable Concrete: Clinker production evaluation. Constr. Build. Mater. 38, 1001–1009. https://doi.org/10.1016/j.conbuildmat.2012.09.061.

Fan, C.C., Huang, R., Hwang, H., Chao, S.J., 2016. Properties of concrete incorporating fine recycled aggregates from crushed concrete wastes. Constr. Build. Mater. 112, 708–715. https://doi.org/10.1016/j.conbuildmat.2016.02.154.

Gebremariam, A.T., Di Maio, F., Vahidi, A., Rem, P., 2020. Innovative technologies for recycling End-of-Life concrete waste in the built environment. Resour. Conserv. Recycl. 163 https://doi.org/10.1016/j.resconrec.2020.104911.

Georget, F., Soja, W., Scrivener, K.L., 2020. Characteristic lengths of the carbonation front in naturally carbonated cement pastes: Implications for reactive transport models. Cem. Concr. Res. 134 https://doi.org/10.1016/j.cemconres.2020.106080.

Goñi, S., Gaztañaga, M. T., & Guerrero, A. (2002). *Role of cement type on carbonation attack*.

K. He X. Zhang S. Ren J. Sun Deep Residual Learning for Image Recognition 2015 10.48550/arXiv.1512.03385.

L.H. Hoong J. D., Lux, J., Mahieux, P. Y., Turcry, P., & Aït-Mokhtar, A. Determination of the composition of recycled aggregates using a deep learning-based image analysis Automation in Construction 116 2020 10.1016/j.autcon.2020.103204.

Hubert, J., Zhao, Z., Michel, F., Courard, L., 2023. Effect of Crushing Method on the Properties of Produced Recycled Concrete Aggregates. Buildings 13 (9), 2217. https://doi.org/10.3390/buildings13092217.

Kim, J., 2022. Influence of quality of recycled aggregates on the mechanical properties of recycled aggregate concretes: An overview. In: Construction and Building Materials, Vol. 328. Elsevier Ltd. https://doi.org/10.1016/j.conbuildmat.2022.127071

Le Saoût, G., Kocaba, V., Scrivener, K., 2011. Application of the Rietveld method to the analysis of anhydrous cement. In: Cement and Concrete Research, Vol. 41(2. Elsevier Ltd., pp. 133–148. https://doi.org/10.1016/j.cemconres.2010.10.003

Li, J., Fang, H., Fan, L., Yang, J., Ji, T., Chen, Q., 2022. RGB-D fusion models for construction and demolition waste detection. Waste Manag. 139, 96–104. https://doi.org/10.1016/j.wasman.2021.12.021.

Li, Y., Liu, W., Xing, F., Wang, S., Tang, L., Lin, S., Dong, Z., 2020. Carbonation of the synthetic calcium silicate hydrate (C-S-H) under different concentrations of CO2: Chemical phases analysis and kinetics. J. CO2 Util. 35, 303–313. https://doi.org/10.1016/j.jcou.2019.10.001.

Liu, G., Li, Q., Song, J., Wang, L., Liu, H., Guo, Y., Yue, G., 2022. Quantitative analysis of surface attached mortar for recycled coarse aggregate. Materials 15 (1). https://doi.org/10.3390/ma15010257.

Lu, B., Shi, C., Cao, Z., Guo, M., Zheng, J., 2019. Effect of carbonated coarse recycled concrete aggregate on the properties and microstructure of recycled concrete. J. Clean. Prod. 233, 421–428. https://doi.org/10.1016/j.jclepro.2019.05.350.

Mazhoud, B., Sedran, T., Cazacliu, B., Cothenet, A., Torrenti, J.M., 2022. Influence of residual mortar volume on the properties of recycled concrete aggregates. Journal of Building Engineering 57. https://doi.org/10.1016/j.jobe.2022.104945.

Melo, C.C.A., Angélica, R.S., Paz, S.P.A., 2020. A proposal for rapid grade control of gibbsitic bauxites using multivariate statistics on XRD data. Miner. Eng. 157 https://doi.org/10.1016/j.mineng.2020.106539.

Moreno-Juez, J., Vegas, I.J., Frías Rojas, M., Vigil de la Villa, R., Guede-Vázquez, E., 2021. Laboratory-scale study and semi-industrial validation of viability of inorganic CDW fine fractions as SCMs in blended cements. Constr. Build. Mater. 271 https://doi.org/10.1016/j.conbuildmat.2020.121823.

Mulder, V.L., Plötze, M., de Bruin, S., Schaepman, M.E., Mavris, C., Kokaly, R.F., Egli, M., 2013. Quantifying mineral abundances of complex mixtures by coupling spectral deconvolution of SWIR spectra (2.1-2.4 μm) and regression tree analysis. Geoderma 207–208 (1), 279–290. https://doi.org/10.1016/j.geoderma.2013.05.011.

Nežerka, V., Zbíral, T., Trejbal, J., 2024. Machine-learning-assisted classification of construction and demolition waste fragments using computer vision: Convolution versus extraction of selected features[Formula presented]. Expert Syst. Appl. 238 https://doi.org/10.1016/j.eswa.2023.121568.

Ouyang, K., Shi, C., Chu, H., Guo, H., Song, B., Ding, Y., Guan, X., Zhu, J., Zhang, H., Wang, Y., & Zheng, J. (2020). An overview on the efficiency of different pretreatment techniques for recycled concrete aggregate. In *Journal of Cleaner Production* (Vol. 263). Elsevier Ltd. https://doi.org/10.1016/j.jclepro.2020.121264.

Pan, Y., Zhang, L., 2021. Roles of artificial intelligence in construction engineering and management: A critical review and future trends. Autom. Constr. 122 https://doi.org/10.1016/j.autcon.2020.103517.

Pedro, D., de Brito, J., Evangelista, L., 2017. Structural concrete with simultaneous incorporation of fine and coarse recycled concrete aggregates: Mechanical, durability and long-term properties. Constr. Build. Mater. 154, 294–309. https://doi.org/10.1016/j.conbuildmat.2017.07.215.

Russakovsky, O., Deng, J., Su, H., Krause, J., Satheesh, S., Ma, S., Huang, Z., Karpathy, A., Khosla, A., Bernstein, M., Berg, A.C., Fei-Fei, L., 2015. ImageNet Large Scale Visual Recognition Challenge. Int. J. Comput. Vis. 115 (3), 211–252. https://doi.org/10.1007/s11263-015-0816-y.

Schneider, C.A., Rasband, W.S., Eliceiri, K.W., 2012. NIH Image to ImageJ: 25 years of image analysis. In Nature Methods (vol. 9 (7), 671–675. https://doi.org/10.1038/nmeth.2089.

Serranti, S., Palmieri, R., Bonifazi, G., Gasbarrone, R., Hermant, G., Bréquel, H., 2023. An Automated Classification of Recycled Aggregates for the Evaluation of Product Standard Compliance. Sustainability 15 (20), 15009. https://doi.org/10.3390/su152015009.

Shen, P., Zhang, Y., Jiang, Y., Zhan, B., Lu, J., Zhang, S., Xuan, D., Poon, C.S., 2022. Phase assemblance evolution during wet carbonation of recycled concrete fines. Cem. Concr. Res. 154 https://doi.org/10.1016/j.cemconres.2022.106733.

Silva, R.V., De Brito, J., Dhir, R.K., 2014. Properties and composition of recycled aggregates from construction and demolition waste suitable for concrete production. Constr. Build. Mater. 65, 201–217. https://doi.org/10.1016/j.conbuildmat.2014.04.117.

Singh, A., 2015. Survey of Noise in Image and Efficient Technique for Noise Reduction. In International Journal of Science and Research (IJSR) ISSN. Www.ijsr.net.

Sivashanmugam, S., Rodriguez, S., Pour Rahimian, F., Elghaish, F., & Dawood, N. (2023). Enhancing information standards for automated construction waste quantification and classification. In *Automation in Construction* (Vol. 152). Elsevier B. V. https://doi.org/10.1016/j.autcon.2023.104898.

Sobotka, A., Sagan, J., 2021. Decision support system in management of concrete demolition waste. Autom. Constr. 128 https://doi.org/10.1016/j.autcon.2021.103734.

Song, Y., Huang, Z., Shen, C., Shi, H., Lange, D.A., 2020. Deep learning-based automated image segmentation for concrete petrographic analysis. Cem. Concr. Res. 135, 106118 https://doi.org/10.1016/j.cemconres.2020.106118.

Stefaniuk, D., Hajduczek, M., Weaver, J.C., Ulm, F.J., Masic, A., 2023. Cementing CO2 into C-S-H: A step toward concrete carbon neutrality. PNAS Nexus 2 (3). https://doi.org/10.1093/pnasnexus/pgad052.

Szeliski, R., 2022. Computer Vision. Springer International Publishing. https://doi.org/10.1007/978-3-030-34372-9.

Tam, V. W. Y., Soomro, M., & Evangelista, A. C. J. (2021). Quality improvement of recycled concrete aggregate by removal of residual mortar: A comprehensive review of approaches adopted. In *Construction and Building Materials* (Vol. 288). Elsevier Ltd. https://doi.org/10.1016/j.conbuildmat.2021.123066.

Tang, B., Fan, M., Yang, Z., Sun, Y., Yuan, L., 2023. A comparison study of aggregate carbonation and concrete carbonation for the enhancement of recycled aggregate pervious concrete. Constr. Build. Mater. 371 https://doi.org/10.1016/j.conbuildmat.2023.130797.

Trotta, O., Bonifazi, G., Capobianco, G., Serranti, S., 2021. Recycling-oriented characterization of post-earthquake building waste by different sensing techniques. *Journal of*. Imaging 7 (9). https://doi.org/10.3390/JIMAGING7090182.

Ulsen, C., Tseng, E., Angulo, S.C., Landmann, M., Contessotto, R., Balbo, J.T., Kahn, H., 2019. Concrete aggregates properties crushed by jaw and impact secondary crushing. J. Mater. Res. Technol. 8 (1), 494–502. https://doi.org/10.1016/j.jmrt.2018.04.008.

Ulsen, C., Contessotto, R., dos Santos Macedo, R., Kahn, H., 2022. Quantification of the cement paste and phase's association in fine recycled aggregates by SEM-based image analysis. Constr. Build. Mater. 320 https://doi.org/10.1016/j.conbuildmat.2021.126206.

Wang, R., Yu, N., & Li, Y. (2020). Methods for improving the microstructure of recycled concrete aggregate: A review. In *Construction and Building Materials* (Vol. 242). Elsevier Ltd. https://doi.org/10.1016/j.conbuildmat.2020.118164.

Wang, B., Yan, L., Fu, Q., & Kasal, B. (2021). A Comprehensive Review on Recycled Aggregate and Recycled Aggregate Concrete. In *Resources, Conservation and Recycling* (Vol. 171). Elsevier B.V. https://doi.org/10.1016/j.resconrec.2021.105565.

Wang, Y., Liu, J., Zhu, P., Liu, H., Wu, C., Zhao, J., 2021b. Investigation of Adhered Mortar Content on Recycled Aggregate Using Image Analysis Method. J. Mater. Civ. Eng. 33 (9) https://doi.org/10.1061/(asce)mt.1943-5533.0003864.

Wang, C., Wu, H., Li, C., 2022a. Hysteresis and damping properties of steel and polypropylene fiber reinforced recycled aggregate concrete under uniaxial low-cycle loadings. Constr. Build. Mater. 319 https://doi.org/10.1016/j.conbuildmat.2021.126191.

Wang, C., Xiao, J., Liu, W., Ma, Z., 2022b. Unloading and reloading stress-strain relationship of recycled aggregate concrete reinforced with steel/polypropylene fibers under uniaxial low-cycle loadings. Cem. Concr. Compos. 131 https://doi.org/10.1016/j.cemconcomp.2022.104597.

Xiao, J.Z., Li, J.B., Zhang, C., 2006. On relationships between the mechanical properties of recycled aggregate concrete: An overview. Materials and Structures/materiaux Et Constructions 39 (6), 655–664. https://doi.org/10.1617/s11527-006-9093-0.

Xu, S., Wang, J., Shou, W., Ngo, T., Sadick, A.-M., Wang, X., 2021. Computer Vision Techniques in Construction: A Critical Review. Arch. Comput. Meth. Eng. 28 (5), 3383–3397. https://doi.org/10.1007/s11831-020-09504-3.

Yang, M.S., Lai, C.Y., Lin, C.Y., 2012. A robust em clustering algorithm for Gaussian mixture models. Pattern Recogn. 45 (11), 3950–3961. https://doi.org/10.1016/j.patcog.2012.04.031.

Zhang, C., Hu, M., Yang, X., Miranda-Xicotencatl, B., Sprecher, B., Di Maio, F., Zhong, X., Tukker, A., 2020. Upgrading construction and demolition waste management from downcycling to recycling in the Netherlands. J. Clean. Prod. 266 https://doi.org/10.1016/j.jclepro.2020.121718.

Zhang, H., Xiao, J., Tang, Y., Duan, Z., Poon, C., sun., 2022. Long-term shrinkage and mechanical properties of fully recycled aggregate concrete: Testing and modelling. Cem. Concr. Compos. 130 https://doi.org/10.1016/j.cemconcomp.2022.104527.